Crustal seismic anisotropy in central Tibet: Implications for deformational style and flow in the crust

A. Arda Ozacar[1,2] and George Zandt[1]

[1] Receiver functions obtained at INDEPTH III stations located near the Bangong-Nujiang suture in central Tibet display a weak Moho signal and strong P to S conversions within the first 5 s that vary systematically with back-azimuth. A single station with representative azimuthal variations located at the sharp onset of strong SKS splitting, is modeled for both dipping layers and seismic anisotropy by using a global minimization technique. Inversion results indicate strong anisotropy (>10%) near the surface and in the middle crust separated by a south-dipping (~25°) layer, possibly related to the earlier phase of crustal shortening. Near-surface anisotropy has a fabric dipping steeply southward and trending WNW-ESE that correlates with the suture and younger strike-slip faults. In contrast, mid-crustal anisotropy occurs in a low-velocity zone and has a fabric dipping gently (~18°) northward that might be related to a well-developed near-horizontal rock fabric induced by crustal flow. *INDEX TERMS:* 7205 Seismology: Continental crust (1242); 7260 Seismology: Theory and modeling; 8102 Tectonophysics: Continental contractional orogenic belts; 8159 Tectonophysics: Rheology—crust and lithosphere; 9320 Information Related to Geographic Region: Asia. **Citation:** Ozacar, A. A., and G. Zandt (2004), Crustal seismic anisotropy in central Tibet: Implications for deformational style and flow in the crust, *Geophys. Res. Lett.*, *31*, L23601, doi:10.1029/2004GL021096.

1. Introduction

[2] The Tibetan plateau is composed of terranes amalgamated along roughly E-W trending sutures [*Yin and Harrison*, 2000] that was subsequently thickened to its present day crustal thickness of ~65 km and uplifted to a mean elevation of ~5 km. The Late Jurassic age Bangong-Nujiang suture (BNS) between the Qiangtang and Lhasa terranes in central Tibet, marks the location of south-to-north variation between the seismically fast, rigid Indian lithosphere and seismically slow, weak Asian lithospheric mantle with increased seismic attenuation [*Barazangi and Ni*, 1982] and strongly developed shear wave anisotropy [*McNamara et al.*, 1994]. Seismic tomography of the upper mantle in this region, revealed a subvertical high velocity zone beneath the northern Lhasa terrane that probably represents the front of detaching Indian mantle lithosphere [*Tilmann et al.*, 2003]. Based on seismic reflection and refraction data, *Zhao et al.* [2001] presented a velocity

model with a 65 ± 5 km thick crust beneath central Tibet that is similar to receiver function (RF) results [*Kind et al.*, 2002].

[3] Seismicity in the region is mainly confined to the upper crust with extension on north trending rifts and slip on conjugate strike-slip faults that probably accommodate eastward spreading of Tibetan crust [*Langin et al.*, 2003; *Taylor et al.*, 2003]. Shear wave splitting results showed a strong polarization anisotropy with fast directions varying from E-W to NE-SW beneath the Qiangtang terrane that emerges over a short distance near the BNS with large split times [*Huang et al.*, 2000]. The strong coherent anisotropy in the north was mainly interpreted in terms of eastward flowing upper mantle, but the sudden occurrence of large anisotropy near the BNS was argued as evidence of significant crustal anisotropy that formed due to strain localization along a lithosphere-penetrating transcurrent shear zone between India and Asia [*Huang et al.*, 2000]. In this paper, we used teleseismic data recorded by the INDEPTH III array spread NNW-SSE across central Tibet (Figure 1), and analyzed the azimuthal dependent variations on RFs at some selected stations to image the crustal structure beneath the suture with constraints on seismic anisotropy and dipping interfaces that help us to distinguish current deformation from fossilized fabrics of older tectonic events and constrain plausible mechanisms of crustal deformation.

2. Receiver Functions at BNS

[4] RFs are typically teleseismic P waveforms that are source-equalized by deconvolving the vertical from the horizontal components and contain isolated P to S conversions produced at seismic impedance contrasts beneath the recording station [*Burdick and Langston*, 1977]. To image the crustal structure across the BNS, we used over 500 high quality P-waveforms from teleseismic earthquakes (M > 5) recorded at seven INDEPTH III stations (see close up view in Figure 1). An iterative time-domain deconvolution algorithm [*Ligorria and Ammon*, 1999] that constructs a RF as a time series sum of Gaussian pulses, is applied with a cut-off frequency of ~1 Hz. After removing poorly deconvolved events, RFs are stacked into 10° back-azimuth and 0.02 s km^{-1} slowness bins for each station. To help assess the continuity of major converted phases, binned RFs from all 7 stations are also stacked together (Figure 2).

[5] In the RF method, presence of dipping layers and/or seismic anisotropy results in rotation of energy out of the source receiver plane that yields patterns of amplitude and arrival times as a systematic function of back-azimuth on both the radial and transverse components. In this data set, the large azimuthally varying polarized phases occur only within the first 5 s and restrict the potential concentration of anisotropy and/or dipping layer to the upper and middle

---

[1]Department of Geosciences, University of Arizona, Tucson, Arizona, USA.
[2]Also at Department of Geological Engineering, Middle East Technical University, Ankara, Turkey.
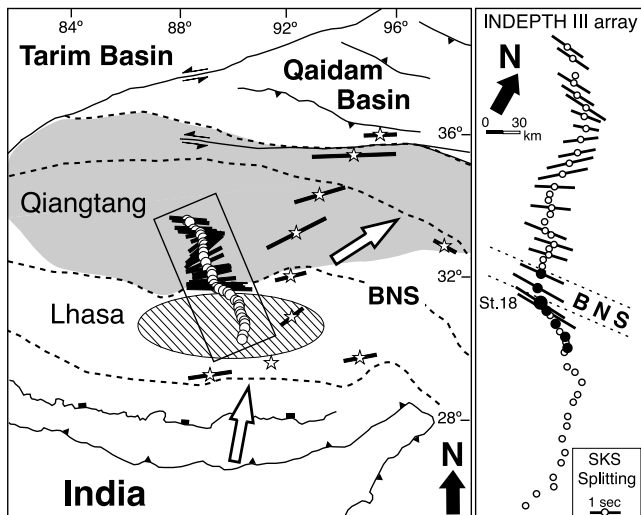
Figure 1. Simplified map of Tibetan plateau (left) and a close up view of INDEPTH III seismic array (right). SKS splitting results are from *Huang et al.* [2000] and *McNamara et al.* [1994]. Zone of inefficient Sn (grey region) is from *Barazangi and Ni* [1982]. Location of subvertical high Vp zone (striped area) is from *Tilmann et al.* [2003]. Sutures (dashed) and major faults (solid) are from *Yin and Harrison* [2000]. Arrows indicate relative plate motions. The stations analyzed in this study are labeled with black circles in the close up view.

crust (Figure 2). Main coherent features observed in the radial RFs include a positive arrival (2.5 s) between two negative arrivals (1.5 s and 3.5 s) and a weak Moho arrival (9 s). The intra-crustal arrivals contain two-lobed transversely polarized energy that peaks at the east and west directions with opposite polarities. Comparison of back-azimuth record sections from each station indicates some variations in the transverse RFs in terms of amplitude reversals and relative time delay patterns that are probably the result of lateral changes in dipping interfaces and plunge directions of anisotropy. The absence of a strong Moho signal contradicts models that require a sharp discontinuity and/or strong seismic anisotropy near the base of the crust.

3. Inversion

[6] We modeled RFs with a cut-off frequency of ~2 Hz from a representative station within the BNS zone, Station 18, located at the edge of sharp onset of strong SKS splitting (Figure 1). Inversion of RFs for crustal seismic structure is a non-linear waveform-fitting problem and linearized techniques can have a strong dependence on the assumed starting model [*Ammon et al.*, 1990]. In order to avoid this problem, we applied the global minimization technique also known as the neighborhood algorithm [*Sambridge*, 1999] that performs directed searches of model parameter space to find a global minimum. Synthetics were computed using a ray-based approach [*Frederiksen and Bostock*, 2000] that allows models to have both anisotropy and dipping layers. Misfits are calculated using cross-correlation which is more sensitive to the arrival times than amplitude based measures [*Frederiksen et al.*, 2002]. This is preferred because the arrival times are more robust than the

amplitudes in RFs [*Ligorria and Ammon*, 1999]. Anisotropy in the layers are restricted to hexagonal symmetry with ellipsoidal phase velocity surfaces but with dipping symmetry axis allowed [*Levin and Park*, 1998]. In the absence of coherent signals from the lower crust, we only modeled arrivals within the first 5 s and assumed a slow-axis anisotropy that can be caused by parallel cracks or alignment of plate shaped minerals (e.g., micas) in metamorphic fabrics [*Weiss et al.*, 1999]. Following *Sherrington et al.* [2004], we used a modified code of *Frederiksen et al.* [2002] to correspond to the parameterization where the anisotropy is assumed to be purely ellipsoidal [*Levin and Park*, 1998]. While free-surface multiples are often observed from high impedance boundaries such as the Moho, intracrustal multiples are much more rarely observed. This is especially the case in tectonically complex crust where heterogeneity and anisotropy have a dissipating effect on the multiples. In addition, multiples are extremely time consuming in the ray-based computations of the synthetics, therefore, we did not include multiples in the modeling technique. This simplifying assumption was tested explicitly in *Sherrington et al.* [2004] for similar data and found to have little effect on the final synthetics.

[7] Considering the potential trade-off between velocity and layer thickness in RFs, it is important to place reasonable constraints using a priori information. In this manner, we determined the number of layers required in the inversion by analyzing the first-order arrivals in the radial component RFs and modeled them first for a 1-D isotropic structure before including dip and anisotropy. We fixed the Vp/Vs ratio to 1.80 in the crust based on the arrival times of Moho multiples [*Kind et al.*, 2002] and inverted for seismic velocity and thickness in each layer by placing limits based on refraction data [*Zhao et al.*, 2001]. Since RFs are sensitive to the velocity contrast between layers, we
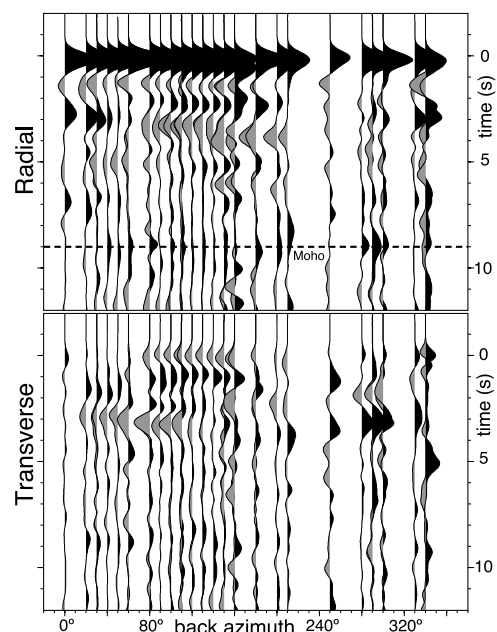
Figure 2. Multiple station stacks of RFs with a cut-off frequency of ~1 Hz. Data is combined from seven INDEPTH III stations located near the BNS (shown in close up view of Figure 1).
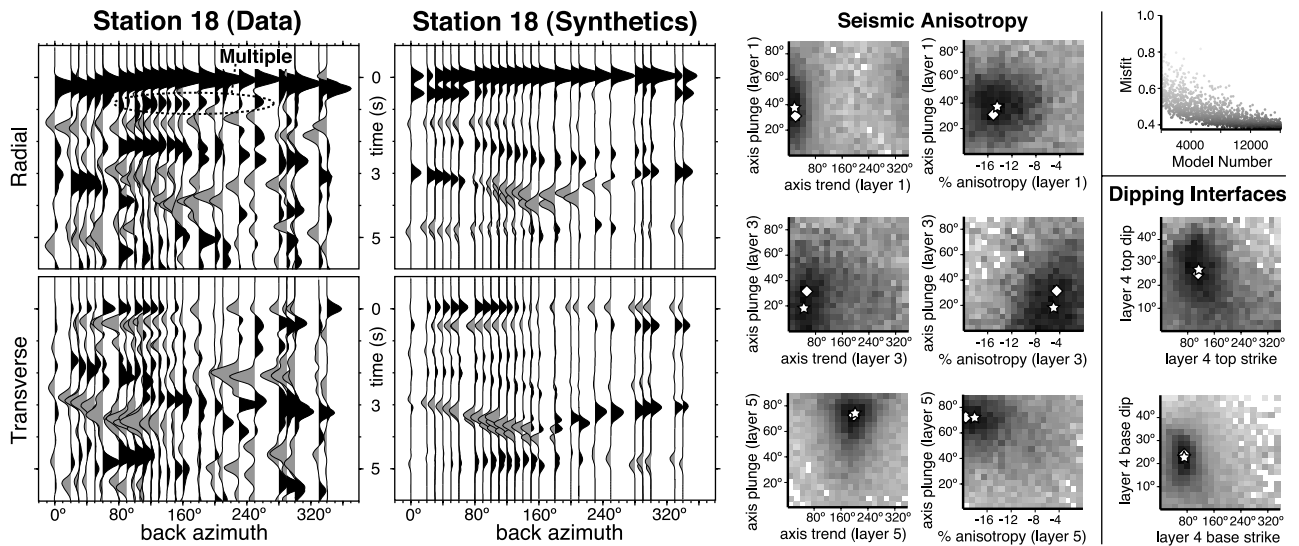
Figure 3. RFs with a cut-off frequency of ~2 Hz at Station 18 and corresponding synthetics for the average model including both dip and anisotropy are at the left. Trade-off curves for plunge/trend of slow axis, percent anisotropy and dip/strike of inclined interfaces are at the right. Dark colors indicate low misfits. Diamonds and stars show the best-fitting and average models.

obtained a six-layer model of alternating low- and high-velocity layers with less resolved absolute values. Next, we performed separate inversion runs allowing dip, anisotropy, and both in different combinations with the aim of matching back-azimuthal variations in both radial and transverse components. Anisotropic models alone provided a poor fit to the observed back-azimuth travel time variations that exceed 1 s in the mid-crust (Figure 3). In contrast, isotropic models with dip improved the traveltime fit but required many dipping interfaces with steep dips and complex geometries. In order to fit the targeted phases with minimal complexity, additional inversion runs were performed for best-fitting anisotropic models with dipping interfaces in the middle crust. Based on these preliminary runs, we limited the inversion to 13 free parameters including degree (percentage) and orientation (plunge and trend) of anisotropy in three isolated low velocity layers and orientation (dip and strike) of the top and bottom interfaces of an isotropic layer in the mid-crust. Then, we carried out a single inversion using over fifteen thousand models and calculated the average of each model parameter by considering all models below a threshold misfit value (Figure 3). The resultant average model was stable and improved the data fit substantially indicating that both anisotropy and interface dip are required to reproduce the major features at Station 18 (Figures 3 and 4). With the available free parameters used in our models we could not fit the amplitudes of some strong arrivals in the data (e.g., Figure 3, transverse component, 2 s, 240 deg.). Although we might be able to fit these arrivals better with additional free parameters, comparing the data with the 7-station stack (Figure 2) suggests the large amplitudes are likely due to local effects and therefore we did not pursue more complex models.

4. Results and Discussion

[8] The average of the best-fitting models for Station 18 indicates strong anisotropy near the surface and in the middle crust, a relatively weak anisotropy at the base of

the upper crust and a south dipping mid-crustal layer (Figure 4). Significant anisotropy (14%) within a near-surface low-velocity layer (0–3 km) has a steeply dipping (>60°S) fabric trending WNW-ESE. The anisotropy recovered within another low-velocity layer at depth range of 10 to 16 km, is weak (5%) and may even be isotropic within the error bounds (Figure 3). Nonetheless, the best fitting model is anisotropic in this layer and although not constrained tightly, still shows orientations (dip: 81°SW, trend: NW-SE) similar to the near surface anisotropy. These shallow fabrics appear to align with the suture and younger
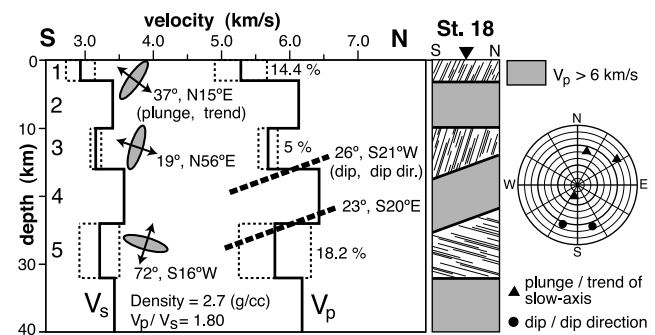
Figure 4. Average crustal seismic velocity model for Station 18 from the inversion allowing both dip and anisotropy to be present. Dotted lines on the velocity profiles indicate the minimum and maximum velocities for the anisotropic layers. Adjacent ellipsis shows the orientation of the rock fabric and the orthogonal arrows the orientation of the symmetry axis. Following convention the orientation of the anisotropy is denoted by the plunge and trend of the symmetry axis. Dark dashed lines indicate the depth and dip of dipping layer interfaces. Schematic crustal column illustrates the location and orientation of fabric within the crust. The adjacent plot shows the plunge and trend of the three anisotropic symmetry axes and the dip and strike of the two dipping layers.

strike-slip faults that merge toward the BNS [*Taylor et al.*, 2003]. Another feature in the model is a pair of roughly E-W striking velocity interfaces with similar southward dip (~25°) at the top (16 km) and bottom (24 km) of an isotropic high velocity layer. This south dipping layer again correlates well with the compression direction and most likely formed in response to an earlier phase of crustal shortening. To summarize, anisotropy and dip within the crust above ~25 km depth are consistent with a combination of inherited and modern structures observed at the surface.

[9] In contrast, anisotropy in the middle crust is again strong (18%) within a low velocity layer (24–32 km), but this time the fabric dips gently (18°) towards the NNE (Figure 4). The top of this anisotropic layer correlates with the starting depth of strong reflectivity that continues to the base of the crust [*Ross et al.*, 2004]. Under these pressure and temperature conditions, it is also possible to have a change in anisotropy shape to fast-axis symmetry that is appropriate for lattice-preferred orientation of minerals. According to synthetic tests, fast and slow axis anisotropy can generate very similar effects in the data when the two axes have opposite trends and supplementary plunges [*Erickson*, 2002]. In such cases, the orientations of the fabric in the slow axis case and the lineation in the fast axis case are the same. Therefore, the gentle dip is unique regardless of whether slow axis or fast axis anisotropy is assumed. The seismic anisotropy results suggest the presence of a near-horizontal foliation or lineation in a ~10 km thick layer in the middle crust of central Tibet. This distinct anisotropy pattern contrasts with both the upper crustal anisotropy and the mantle shear wave splitting fast polarization directions [*Huang et al.*, 2000], suggesting a ductile deformation that will decouple the middle crust from above and below. The most likely explanation for the observed mid-crustal anisotropy is that a ~N-S directed flow within a sub-horizontal low viscosity channel is responsible for producing the nearly horizontal rock fabric, perhaps by aligning mica minerals. This hypothesis agrees with the boundary forces of subducting Indian lithosphere and implies elevated crustal temperatures consistent with the shallow seismicity [*Langin et al.*, 2003]. Analysis of RFs from other stations [*Sherrington et al.*, 2004] and regional surface wave dispersion across the Tibetan plateau also require mid-crustal anisotropy [*Shipiro et al.*, 2004], consistent with our results, and suggest a widespread phenomenon.

[10] Finally, we generated synthetic waveforms for SKS-wave splitting through the Station 18 anisotropic crustal model and calculated maximum split times <0.5 s. The observation of minor variations in the crustal RFs between stations that have dramatically different teleseismic splitting measurements and the relatively small effect of our crustal anisotropy model on synthetic SKS split times indicates the observed splitting measurements in excess of 2 s in this region [*Huang et al.*, 2000] are most likely due to mantle structure. Modeling of shear wave splitting for 2D mantle models with vertical boundaries between anisotropic domains indicates that it is possible to jump from null observations to split times in excess of 1 s over very short distances [*Rumpker and Ryberg*, 2000].

References

Ammon, C. J., G. E. Randall, and G. Zandt (1990), On the nonuniqueness of receiver function inversions, *J. Geophys. Res.*, *95*, 15,303–15,319.

Barazangi, M., and J. Ni (1982), Velocities and propagation characteristics of *Pn* and *Sn* beneath the Himalayan Arc and Tibetan Plateau: Possible evidence for underthrusting of Indian continental lithosphere beneath Tibet, *Geology*, *10*, 179–185.

Burdick, L. J., and C. A. Langston (1977), Modeling crustal structure with converted phases in teleseismic body-waveforms, *Bull. Seismol. Soc. Am.*, *67*, 677–691.

Erickson, J. (2002), Anisotropic crustal structure inversion using a niching genetic algorithm: A feasibility study, M.S. thesis, Univ. of Ariz., Tucson.

Frederiksen, A. W., and M. G. Bostock (2000), Modeling teleseismic waves in dipping anisotropic structures, *Geophys. J. Int.*, *141*, 401–412.

Frederiksen, A. W., H. Folsom, and G. Zandt (2002), Neighborhood inversion of teleseismic *Ps* conversions for anisotropy and layer dip, *Geophys. J. Int.*, *155*, 200–212.

Huang, W., et al. (2000), Seismic polarization anisotropy beneath the central Tibetan Plateau, *J. Geophys. Res.*, *105*, 27,979–27,989.

Kind, R., et al. (2002), Seismic images of crust and upper mantle beneath Tibet: Evidence for Eurasian plate subduction, *Science*, *298*, 1219–1221.

Langin, W. R., L. D. Brown, and E. A. Sandvol (2003), Seismicity of central Tibet from project INDEPTH III seismic recordings, *Bull. Seismol. Soc. Am.*, *93*, 2146–2159.

Levin, V., and J. Park (1998), P-SH conversions in layered media with hexagonally symmetric anisotropy: A cookbook, *Pure Appl. Geophys.*, *151*, 669–697.

Ligorria, J. P., and C. J. Ammon (1999), Iterative deconvolution and receiver-function estimation, *Bull. Seismol. Soc. Am.*, *89*, 1395–1400.

McNamara, D. E., et al. (1994), Shear wave anisotropy beneath the Tibetan Plateau, *J. Geophys. Res.*, *99*, 13,655–13,665.

Ross, A. R., et al. (2004), Deep reflection surveying in central Tibet: Lower crustal layering and crustal flow, *Geophys. J. Int.*, *156*, 115–128.

Rumpker, G., and T. Ryberg (2000), New ''Fresnel-zone'' estimates for shear-wave splitting observations from finite-difference modeling, *Geophys. Res. Lett.*, *27*(13), 2005–2008.

Sambridge, M. (1999), Geophysical inversion with a neighborhood algorithm: I. Searching a parameter space, *Geophys. J. Int.*, *138*, 479–494.

Shipiro, N., et al. (2004), Thinning and Flow of Tibetan crust constrained by seismic anisotropy, *Science*, *305*, 233–236.

Sherrington, H. F., G. Zandt, and A. Frederiksen (2004), Crustal fabric in the Tibetan Plateau based on waveform inversions for seismic anisotropy parameters, *J. Geophys. Res.*, *109*, B02312, doi:10.1029/2002JB002345.

Taylor, M., et al. (2003), Conjugate strike-slip faulting along the Bangong-Nujiang suture zone accommodates coeval east-west extension and north-south shortening in the interior of the Tibetan Plateau, *Tectonics*, *22*(4), 1044, doi:10.1029/2002TC001361.

Tilmann, F., J. Ni, and INDEPTH III Seismic Team (2003), Seismic imaging of the downwelling Indian lithosphere beneath central Tibet, *Science*, *300*, 1424–1427.

Weiss, T., et al. (1999), Seismic velocities and anisotropy of the lower continental crust: A review, *Pure Appl. Geophys.*, *156*, 97–122.

Yin, A., and T. M. Harrison (2000), Geologic evolution of the Himalayan-Tibetan orogen, *Annu. Rev. Earth Planet. Sci.*, *28*, 211–280.

Zhao, W., et al. (2001), Crustal structure of central Tibet as derived from project INDEPTH wide-angle seismic data, *Geophys. J. Int.*, *145*, 486–498.

A. A. Ozacar and G. Zandt, Department of Geosciences, University of Arizona, Tucson, AZ 85721-0077, USA. (ozacar@geo.arizona.edu; zandt@geo.arizona.edu)